

A Biomass Gasifier Including An Ionic Transport Membrane System For Oxygen Transfer

Tania Antonini*, Katia Gallucci, Pier Ugo Foscolo

Industrial Engineering Department, University of L'Aquila, Via G. Gronchi, 18 - 67100 L'Aquila, Italy
tania.antonini@graduate.univaq.it

Ion transport membrane (ITM) reactors have been suggested as a novel technology for fuel reforming and oxy-fuel combustion, integrating air separation and fuel conversion, in order to reduce plant complexity and the associated energy penalty (Hong et al., 2012). The presence of a fuel on the permeate side helps increasing oxygen chemical potential gradient across the membrane and oxygen permeation rates.

This paper addresses the field of fluidized bed biomass gasification: a globally endothermic process, requiring oxygen input to the reactor to assure autothermal behaviour. It is proposed to incorporate ITM in a biomass gasifier and a model is developed to study partial combustion of char as a means to provide thermal energy to the gasification reactions. Reference is made to a lab scale gasification rig: the gasifier temperature is imposed, and conservation equations are integrated across the fluidized bed close to the membrane. Char concentration is considered uniform everywhere, so that the reaction rate depends on local temperature and oxygen concentration. A pseudo-homogeneous reaction model is considered. The approach of interpenetrating continua is utilized to schematize the gas/solid fluidized bed properties.

The numerical evaluations show that oxygen transfer fluxes of the order of those exhibited experimentally by perovskite membranes, in the temperature range typical for fluidized bed gasifiers, can assure process feasibility and autothermal behaviour, without diluting the product gas with nitrogen, compressing air streams or adopting complex reactor schemes.

1. Introduction

The world's energy system needs to be adapted into a more sustainable one, based on a diverse mix of energy sources, in particular renewables and among them biomass, enhancing power generation efficiency, addressing the pressing challenges of security of supply and climate change, whilst increasing the competitiveness of *green* power systems. Bio-energy is amenable to distributed power production, close to areas of biomass availability, and energy market deregulation.

In the quite broad scenario of power, and combined heat and power (CHP), from biomass, the route of advanced biomass gasification systems offers good perspectives for cost-effective industrial applications and high potential for further improvements: maximizing syngas yield, optimizing gas quality, increasing gas purity, and above all increasing the overall process efficiency. Advanced innovative process integration and combination concepts aim to achieve these goals.

Dense perovskite membranes can exhibit high oxygen ion permeability at elevated temperatures when subjected to a gradient of oxygen chemical potential (Xu and Thomson, 1999). This behaviour is generally attributed to the partial substitution of both A and B cations in the ABO_3 structure and the formation of oxygen vacancies (Teraoka et al., 1988). Their motion gives rise to oxygen perm-selectivity and transport of electric charges is compensated by the transport of electron-holes in the reverse direction. Recent, substantial improvements in the membrane preparation technologies on relatively large scale (Vito, 2013) and in the oxygen permeation fluxes in the 850 – 1000°C temperature range (Anzoletti, 2014) would allow their application to a biomass gasifier.

Char combustion is one of the most important chemical reactions taking place inside a gasifier, providing practically all the thermal energy needed for the endothermic reactions. Oxygen supplied to the gasifier reacts with the combustible substances present, resulting in the formation of CO_2 and H_2O , which

subsequently undergo reduction upon contact with the pyrolysis products. An alternative combustion reaction is the oxidation of hydrogen in the fuel to produce steam (Basu, 2006). Homogeneous and catalytic oxidation processes resulting from coupling oxygen permeation through a membrane and fuel gas burning were already studied in the literature (Hong et al., 2013).

2. Model description

A case of study is assumed (Rapagnà et al, 2009), as summarized in Table 1. Cylindrical ITM pipes (Table 2) are supposed to be immersed vertically inside the fluidized bed and connected by an input and output air collector (Figure 1). Particles are considered uniformly dispersed in the bed layer surrounding each pipe. Air at atmospheric pressure flows inside each pipe. A tentative, average value is first assumed for the oxygen permeation flux at the operating conditions, J_{O_2} , referred to the average permeation surface of each tubular membrane:

$$A_m = \pi \cdot d_m \cdot L, \quad d_m = \frac{2 \cdot t}{\ln[(d_o)/d_{io}]} \quad (1)$$

The knowledge of the gasifier total oxygen demand allows to fix the inlet air flow rate, Q_{air} , and a preliminary system configuration is obtained choosing the air superficial velocity inside each ITM pipe.

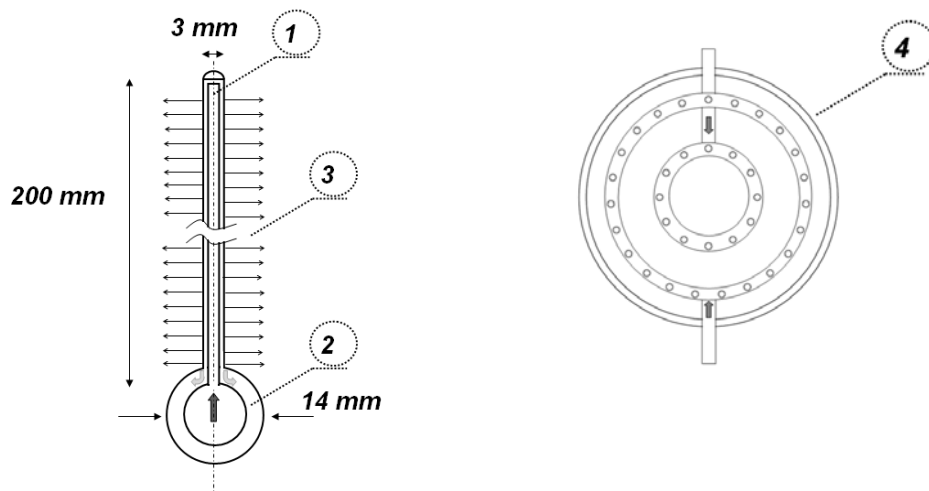


Figure 1: (1) longitudinal section of a membrane pipe with its feeding capillary; (2) cross section of the inlet and outlet air collector; (3) oxygen permeation surface; (4) layout of the whole oxygen permeation system

Table 1: Parameter values characterizing the gasifier assumed as a case of study in this paper

Bed material	Olivine sand	Gas average composition [% by volume]			
Average particle diameter, d_p [μm]	400	H ₂	35	CO	14
Particle density, ρ_p [kg/m^3]	2500	CO ₂	14	CH ₄	7
Average bed voidage, ϵ	0.5	H ₂ O	30		
Bed temperature, T_B [$^{\circ}\text{C}$]	850	Char fraction in the bed, [% by weight]			2, 4, 6
Equivalence ratio, ER	0.25	Char particle density, ρ_c [kg/m^3]			300
Biomass elemental composition (dry, ash free – daf) [%by weight]		Average char particle diameter, d_c [μm]			800
Carbon	50	Oxygen demand per kg of daf biomass (ER*=0.25):			
Hydrogen	6	F _{O₂} [Nl/kg daf]			240.5
Oxygen	44				

* ER (equivalence ratio): oxygen demand divided by what would be needed for complete biomass combustion.

Table 2: Specifics of ITM pipes

Length of each pipe, L [mm]	200
Number of pipes, N	35
Inside diameter, d_{io} [mm]	2.4
Air adduction capillary, d_i [mm]	1.6
Thickness, t [mm]	0.3
Air inlet superficial velocity, u_{in} [m/s]	5

Oxygen depletion balance in the air stream inside each membrane pipe:

$$\frac{dn_{O_2}}{dz} = -J_{O_2} \cdot a_m; \quad a_m = \pi \cdot d_m \quad (2)$$

$$\text{Boundary condition: } N \cdot n_{O_2} = Q_{air} \cdot P / (R \cdot T) \cdot y_{O_2in} \text{ at } z = 0 \quad (3)$$

2.1 Constitutive equations to determine the oxygen permeation flux

Three oxygen transfer resistances in series are considered and local steady state conditions are imposed: the radial oxygen flow from the bulk of the air stream to the membrane inner surface is equal to the oxygen permeation rate across the membrane and additionally to the O_2 flow rate reaching the fluidized bed at its outer surface.

1. Oxygen mass transfer from the air feed stream to the membrane surface:

$$J_{O_2} = k_g / (R \cdot T) \cdot (P_{O_2}^a - P_{O_2}^l) \cdot (d_{io} / d_m) \quad (4)$$

where the mass transfer coefficient, k_g , is estimated by means of literature correlations (Treybal, 2003).

2. Adsorption onto the membrane surface, dissociation and ionization of oxygen molecules and subsequent incorporation of the ions into the lattice vacancies (feed side surface exchange) of the perovskite membrane; transport of lattice oxygen ions through the membrane (bulk diffusion); association of lattice oxygen ions to oxygen molecules and desorption from the membrane surface into the gas phase (permeate side surface exchange). The overall oxygen flux is given by the following equation obtained by Tan and Li (2002) who adapted to the case of capillary membranes the oxygen transport model originally proposed by Xu and Thomson (1999) for flat membranes:

$$J_{O_2} = [D_V \cdot k_r \cdot (P_{O_2}^{I,0.5} - P_{O_2}^{II,0.5})] / \left[2 \cdot t \cdot k_f (P_{O_2}^I \cdot P_{O_2}^{II})^{0.5} + \frac{d_m}{d_{io}} \cdot D_V \cdot (P_{O_2}^{II})^{0.5} + \frac{d_m}{d_o} \cdot D_V \cdot (P_{O_2}^I)^{0.5} \right] \quad (5)$$

Each of the parameters in the above equation (D_V , k_r and k_f) is expressed as a function of temperature by means of an Arrhenius type equation. In Table 2, pre-exponential factor and activation energy values are reported, as found by Xu and Thomson (1999). As far as k_r is concerned, in Table 2 are also reported corresponding values derived from fitting experimental data of oxygen permeation flux through thin tubular perovskite membranes recently obtained at the Eindhoven Technical University, the Nederland (Anzoletti, 2014): the reduction in the pre-exponential factor and activation energy indicate that newly developed membranes are characterized by substantially greater permeability and are activated at relatively lower temperatures.

Table 2: Pre-exponential factor and activation energy values for the parameters in equation (5)

Parameter	Pre-exponential factor	Activation Energy, E_A [kJ/mol]
D_V [cm ² /s]	$1.58 \cdot 10^{-2}$	73.6
k_f [cm/atm ^{0.5} /s]	$5.90 \cdot 10^6$	226.8
k_r [mol/cm ² /s]	$2.07 \cdot 10^4$	241.3
k_r [mol/cm ² /s] (Anzoletti, 2014)	0.488	108.2

3. Oxygen mass transfer in the fluidized bed, enhanced by simultaneous char combustion.

The char combustion process is comparatively *fast* with respect to oxygen diffusion in the fluidized bed, so that O_2 is almost completely consumed in a fluidized bed layer close to the membrane surface (sweep side). The global combustion reaction rate, r_c (char moles burnt per unit time and fluidized bed volume) is assumed to depend linearly on the local oxygen concentration:

$$r_c = k_o \cdot C_{O_2}; \quad 1/k_o = 1/k_c \cdot a_c + 1/(k \cdot \rho_{M,char} / \rho_{M,gas}) \quad (6)$$

where the oxygen mass transfer coefficient in the gaseous phase surrounding the particle (k_c) can be estimated by means of the Frössling correlation (Fogler, 1992), adopting the conservative assumption that the relative velocity between char particles and gas phase is zero.

The global kinetic constant, k_o , takes into account intrinsic reaction rate (Kashiwagi and Nambu, 1992) and diffusion phenomena at the char particle level (Di Blasi, 2000). The experimental results of thermal gravimetric tests performed at ambient pressure and four different oxygen concentrations (in the range 0.21 – 0.0028 oxygen molar fraction) indicated that the char oxidation process could well be expressed by an overall one-step first-order reaction, where char is considered to be pure carbon ($C + O_2 \rightarrow CO_2$).

In the fluidized bed gasifier char particles are relatively small (Table 1), nevertheless Eq(6) allows to predict that a diffusion-controlled combustion regime is established above $T_B = 740^\circ\text{C}$, because the mass transfer rate coefficient, $a_c k_c$, is small compared to the reaction rate constant, $k \rho_{M,char} / \rho_{M,gas}$.

As far as oxygen transfer from the membrane surface to the fluidized bed is concerned, in a pseudo-homogeneous description the diffusion coefficient is obtained as the bulk diffusion in the gas mixture inside the gasifier corrected for the shading and tortuosity effects due to the presence of particles; in analogy to the random pore model widely utilized for porous catalysts (Smith, 1981), the following relation is utilized:

$$D_{O_2}^e = D_{O_2} \cdot \varepsilon^2 \quad (7)$$

The condition of zero oxygen accumulation at the membrane/fluidized bed interface results in the following relation expressing the equality between the oxygen flow transported by the membrane and that diffusing toward the fluidized bed:

$$J_{O_2} \cdot d_m = -\rho_{M,gas} \cdot D_{O_2}^e \cdot \left(\frac{dy_{O_2}}{dr} \right) \cdot 2r \text{ at } r = d_o/2 \quad (8)$$

To evaluate the RHS of the above equation, the oxygen concentration profile should be obtained by integration of the differential, stationary mol balance:

$$\rho_{M,gas} \cdot D_{O_2}^e \cdot \frac{d}{dr} \cdot \left[r \cdot \left(\frac{dy_{O_2}}{dr} \right) \right] = r \cdot r_c \quad (9)$$

The product $\rho_{M,gas} \cdot D_{O_2}^e$ can be reasonably considered constant in this study because temperature fluctuates no more than 3% of its absolute value in the fluidized bed, T_B , as it will be shown later.

$$\text{Boundary conditions: } r = \frac{d_o}{2} \rightarrow y_{O_2} = P_{O_2}^I/P \quad r = \infty \rightarrow y_{O_2} = y_{O_2,bulk} = 0 \quad (10)$$

The behaviour of the fluidized bed reactor can be reasonably approximated by a perfect mixer, so that the oxygen bulk concentration is assumed constant and equal to that in the outlet gas stream: according to experimental evidence, this value is zero for a biomass gasifier that operates in a reducing atmosphere.

The above Eqns (4), (5), (8) allow to determine the oxygen flux, J_{O_2} , and the oxygen partial pressure on both sides of the membrane, $P_{O_2}^I$ and $P_{O_2}^{II}$, at a given height, z , of the tubular membrane element, under isothermal conditions. The integration along z of Eq(8) then allows to determine the overall oxygen flow rate transferred to the gasifier. A complete description of the oxygen transport system is finally obtained iterating calculations till the required overall oxygen flow to the gasifier and optimum membrane transport system configuration is obtained.

Combustion of char determines a temperature increase in the fluidized bed layer attached to the membrane surface, above that in the bulk of the bed. To estimate the importance of this temperature perturbation, reference is made here to the air entrance section, where the oxygen transport rate is the highest, and it is assumed that heat exchange between the fluidized bed and the membrane is negligible: such adiabatic condition would correspond to the maximum temperature gap that may develop on the permeate side, between the membrane itself and the bulk of the fluidized bed.

It is considered that the thermal energy generated by combustion of char is transferred by thermal conductivity:

$$k_t^e \cdot \frac{d}{dr} \cdot \left[r \cdot \left(\frac{dT}{dr} \right) \right] = \Delta H_r \cdot r \cdot r_c \quad (11)$$

$$\text{Boundary conditions: } r = \frac{d_o}{2} \rightarrow T = T_W \quad r = \infty \rightarrow T = T_B \quad (12)$$

With reference to the latter boundary condition, in the numerical integration it has in fact been assumed that temperature reaches the value in the bulk of fluidized bed (T_B) at a distance from the membrane corresponding to complete consumption of oxygen, that is very close to the permeation interface: fluidized bed reactors are characterized by a strong tendency to smooth rapidly temperature differences.

The equivalent thermal conductivity of the fluidized bed is obtained from the corresponding values of gas and solid phases (Smith, 1981):

$$k_t^e = k_{tg}^e \cdot k_{ts}^{1-\varepsilon} \quad (13)$$

It has been shown in the literature (Chen and Chen, 1981) that taking into account the contribution of radiative heat transfer in Eq.11 would determine an additional 10-20% of the overall heat transfer capacity between an immersed pipe and the fluidized bed. The next step in this investigation will be an experimental study to validate, among other assumptions made in the model, the choice to neglect this radiative term that in any case would contribute to flatten the temperature profile.

When the system of Eq.9 and Eq.11 with corresponding boundary conditions is integrated with reference to the inlet cross section ($z = 0$) of the tubular membranes, combined oxygen concentration and temperature profiles in the fluidized bed layer at the membrane surface can be estimated for comparison with the isothermal case.

3. Results and discussion

The model described above was implemented in MATLAB®, and calculations were performed with reference to the membrane geometry illustrated in Figure 1 and parameter data reported in Table 1.

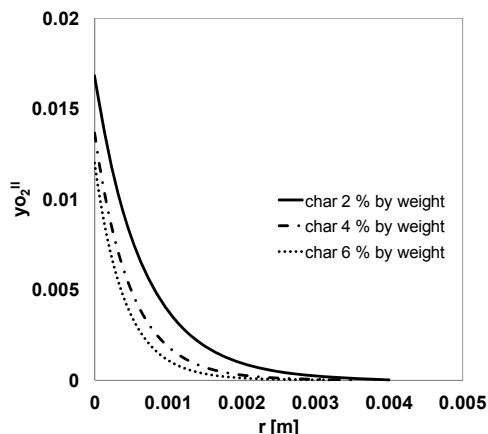


Figure 2: O_2 concentration in the fluidized bed as a function of the radial distance from the membrane surface; $T=T_B$

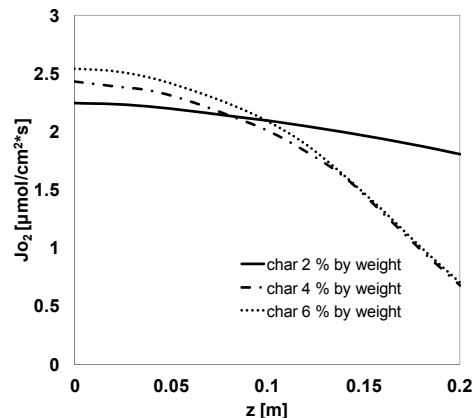


Figure 3: O_2 flux referred to the membrane average diameter as a

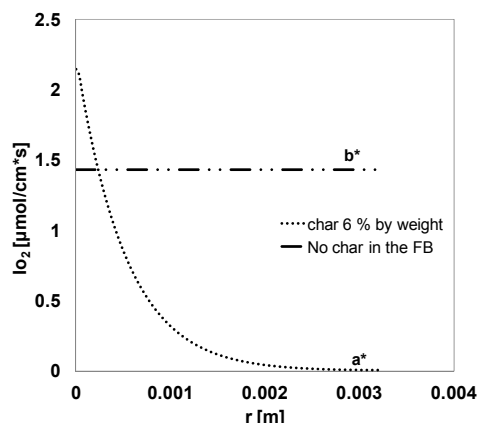


Figure 4: O_2 flow rate per unit membrane height as a function of the radial distance from the membrane surface; a^* : when 6% of char is present in the FB, b^* : when no char is present in the FB

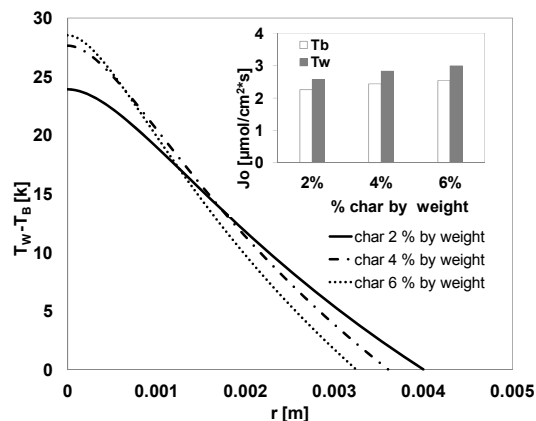


Figure 5: Temperature profile as a function of the radial distance from the membrane surface ($z=0$); comparison of oxygen flux calculated at $T=T_B$ and $T=T_W$, respectively

Figure 2 shows the oxygen molar fraction in the fluidized bed (FB) as a function of the radial distance from the membrane outer surface, with reference to the head of the membrane pipe ($z = 0$). It is confirmed that the O_2 concentration becomes negligible at a distance equal to or less than the membrane external diameter ($d_0 = 3$ mm): the greater the char concentration, the steeper is the O_2 concentration profile, because the combustion reaction rate is faster.

In Figure 3, the oxygen permeation flux across the membrane (referred to its average diameter) is shown, as a function of the membrane height, z . Reduction of flux between the inlet and outlet sections is only about 15% with the lowest char concentration, although oxygen in the air stream is reduced by about 50%: O_2 partial pressure on the feed side affects slightly the permeation rate, so that the oxygen input to the gasifier is quite uniform along the membrane pipe. With higher char concentrations, however, a very different behaviour is predicted due to the prevailing effect of oxygen exhaustion in the air stream.

Figure 4 shows the importance of the fast combustion reaction on the permeate side, in comparison to a purely diffusion process: the oxygen flow rate per unit membrane length, I_{O_2} , is reported as a function of the radial distance from the membrane surface. The presence of char helps increasing the oxygen flow coming out of the membrane surface, which is then extinguished over a very short distance in the fluidized bed. When char is absent, the flow of oxygen towards the bulk of the fluidized bed is of course constant.

Finally, Figure 5 allows to estimate quantitatively the temperature perturbation brought about by the exothermic char combustion reaction: in the air inlet section, the membrane temperature increases slightly above that in the bulk of the fluidized bed, however membrane permeability is a strong function of temperature because of the Arrhenius-type dependency law.

4. Conclusions

The model developed in this study is able to capture correctly major features of oxygen transfer to a fluidized bed gasifier by means of ionic transport membranes, with the scope to burn char therein and provide the energy input required by autothermal gasification processes. When the temperature of the gasifier is set at industrially relevant conditions (850°C), satisfactory oxygen permeation fluxes are predicted, enough to accommodate the whole bundle of membrane pipes inside the gasifier. A preliminary estimate of the effect of temperature perturbation due to char combustion at the membrane surface indicates that the associated increase in permeability is substantial: therefore the next step in the model upgrading will be coupling an energy conservation relationship to the oxygen balance.

Symbols

a_c	char particle surface per unit bed volume [m^2/m^3]	$P_{O_2}^a$	O_2 partial pressure in the air stream [atm]
A_m	average membrane O_2 permeation area [mm^2]	$P_{O_2}^I$	O_2 partial pressure on retentate side [atm]
C_{O_2}	O_2 volumetric molar concentration [$kmol/m^3$]	$P_{O_2}^{II}$	O_2 partial pressure on permeate side [atm]
D_{O_2}	O_2 diffusion coefficient [m^2/s]	Q_{air}	inlet air flow rate [m^3/s]
$d_{i,i,o,m}$	characteristic diameters of ITM system [mm]	R	gas-law constant [-]
D_v	O_2 vacancy bulk diffusion coefficient [cm^2/s]	r	radial coordinate [m]
J_{O_2}	O_2 permeation flux [$\mu mol/cm^2/s$]	r_c	char combustion rate [$mol/m^3/s$]
k, k_o	kinetic constants [1/s]	t	membrane thickness [mm]
k_c, k_g	mass transfer coefficients [m/s]	T_B, T_w	bed and membrane temperature [°C]
k_f	forward surface exchange rate constant [$cm/atm^{0.5}/s$]	y_{O_2}	oxygen molar fraction [-]
k_r	reverse surface exchange rate constant [$mol/cm^2/s$]	z	axial coordinate [m]
k_t	thermal conductivity [$W/m^\circ C$]	ΔH_r	reaction enthalpy [kJ/mol]
L	length of each ITM pipe [mm]	ϵ	average fluidized bed voidage [-]
N	number of tubular ITM pipes [-]	$\rho_{M,char}$	char molar density [mol/m^3]
n_{O_2}	O_2 molar flow rate on retentate side [$\mu mol/s$]	$\rho_{M,gas}$	gas phase molar density [mol/m^3]

References

- Anzoletti V., 2014 MSc Dissertation in Chemical Engineering, University of L'Aquila, Italy.
- Basu P., 2006, Combustion and gasification in fluidized beds, Taylor & Francis Group, London, United Kingdom, ISBN: 0-8493-3396-2.
- Blasi C.D., 2000, Dynamic behaviour of stratified downdraft gasifiers, Chem. Eng. Sci., 55, 2931-2944.
- Chen J.C., Chen K.L., 1981, Analysis of simultaneous radiative and conductive heat transfer in fluidized beds, Chem. Eng. Commun., 9, 255-271.
- Fogler H.S., 1992, Elements of chemical reaction engineering, Prentice-Hall, Inc., Englewood Cliffs, New Jersey, ISBN: 0-13-1253220-4.
- Hong J., Kirchen P., Ghoniem A.F., 2012, Numerical simulation of ion transport membrane reactors: Oxygen permeation and transport and fuel conversion, J. Membr. Sci., 407-408, 71-85.
- Hong J., Kirchen P., Ghoniem A.F., 2013, Interactions between oxygen permeation and homogeneous-phase fuel conversion on the sweep side of an ion transport membrane, J. Membr. Sci., 428, 309-322.
- Kashiwagi T., Nambu H., 1992, Global kinetic constants for thermal oxidative degradation of a cellulosic paper, Combust. Flame, 88, 345-368.
- Rapagnà S., Gallucci K., Di Marcello M., Foscolo P.U., Nacken M., Heidenreich S., 2009, In situ catalytic ceramic candle filtration for tar reforming and particulate abatement in a fluidized-bed biomass gasifier, Energy & Fuels, 23, 3804-3809.
- Smith J.M., 1981, Chemical Engineering Kinetics, McGraw Hill Chem. Eng. Series, Tokyo, Japan, ISBN: 0-07-066574-5.
- Tan X., Li K., 2002, Modeling of Air Separation in a LSCF Hollow-Fiber Membrane Module, AIChE J., 48, 1469-1477.
- Teraoka Y., Zhang H.M., Okamoto K., Yamazoe N., 1988, Mixed ionic-electronic conductivity of $La_{1-x}Sr_xCo_{1-y}Fe_yO_{3-\delta}$ perovskite-type oxides, Mat. Res. Bull., 23, 51-58.
- Treybal R.E., 2003, Mass transfer operations, McGraw Hill, Nirali, India, ISBN: 0-07-066615-6
- VITO (Vision on technology), 2013, Catalogue Materials Technology, <www.vito.be>, Accessed 05.12.2013.
- Xu S.J., Thomson W.J., 1999, Oxygen permeation rates through ion-conducting perovskite membranes, Chem. Eng. Sci., 54, 3839-3850.